

Effect of Grain Size on Corrosion Properties of Low Alloy Steel under H₂S/CO₂ Environment

Hongwei Wang^{1,*}, Chi Yu²

¹ School of Control Engineering, Northeastern University at Qinhuangdao, Qinhuangdao 066004, China;

² School of Resources and Materials, Northeastern University at Qinhuangdao, Qinhuangdao 066004, China

*E-mail: wanghw0819@163.com

Received: 28 November 2016 / Accepted: 27 February 2017 / Published: 12 April 2017

The corrosion properties of low alloy steel immersed in NaCl solution containing H₂S and CO₂ are investigated. The study is carried out using electrochemical measuring method. Scanning electron microscopy is used to observe the corrosion surface morphology, and the compositions are analyzed by energy-dispersive spectroscopy. The results show that the low alloy steel with more fine grain shows good corrosion resistance, it has lower corrosion current density and bigger the polarization resistance. The relationship of rolling parameters, grain size, electrochemical parameters and corrosion surface morphology are discussed.

Keywords: low alloy steel; H₂S/CO₂; electrochemical measurements; grey system theory

1. INTRODUCTION

The low alloy steel not only need excellent mechanical property, but also has well corrosion resistance for oil and gas industry. The special work conditions with amount of H₂S and CO₂ are prone to cause corrosion failure, which will bring serious accident and economic loss. So it is necessary to develop low alloy steel and study the corrosion property.

The corrosion problems about H₂S/CO₂ have been studied [1-5]. As the development of oil field with high H₂S content, the environment will become worse and worse, the corrosion behavior is poorly understood. Pots et al. [6] propose a critical ratio of P_{H_2S}/P_{CO_2} to understand the corrosion behavior, when $P_{H_2S}/P_{CO_2} > 500$, CO₂ plays an important role during corrosion process, when $P_{H_2S}/P_{CO_2} < 20$, H₂S has a major influence, and $20 < P_{H_2S}/P_{CO_2} < 500$, the corrosion behavior is controlled by H₂S and CO₂ simultaneously. Li et al. [4] research the corrosion properties of tubing

steel in environment with high H₂S and CO₂ content, and the results indicate that H₂S has an important influence on the whole reaction process and precipitation of iron sulfide on the steel surface is superior to iron carbonate. Zhao et al. [7] study the corrosion behavior about Ni-based alloys in simulation solution containing H₂S/CO₂ at different temperature. Wang et al. [8] investigate the effects of alloy elements Cr on corrosion resistance in CO₂/H₂S environment. Their studies are focused on the characterization by accelerated corrosion method.

However, the corrosion behavior of alloy steel under H₂S/CO₂ environment is an electrochemical process, the technique has been widely used to study the corrosion mechanism and has been proven to be effective [9-14]. Some results are obtained, mainly for single CO₂ environment [15-17] or H₂S environment [18-22]. Very few studies under the H₂S/CO₂ coexistence conditions are reported [23-28]. Zhang et al. [23] study the corrosion behavior of carbon steel under dynamic high pressure H₂S and CO₂ environment, the results show the corrosion process switches to H₂S corrosion control with the increase of partial pressure ratio. Wu et al. [24] investigate influence of chromium on mechanical properties and corrosion behavior of P110 grade tube steel under H₂S and CO₂ environment ($P_{CO_2}/P_{H_2S}=15$) at 60°C, the total pressure is 0.1 MPa, the results show the corrosion rate is reduced due to the rise of Cr element by the polarization curve and electrochemical impedance spectroscopy. Wang et al. [25] and Yan et al. [27] research the corrosion behavior of different types of materials. Wang et al [26] study the relationship between the corrosion rate and immersion time of low alloy steel. However, grain size has a strong impact on corrosion behavior, and the problem is always not also reported by the electrochemical method.

In this paper, the corrosion properties of low alloy steel under 3.5 wt% NaCl solution containing H₂S/CO₂ are studied to simulate the practical working environment of oil and gas industry, ($P_{CO_2}/P_{H_2S}=7$) at 75°C, the total pressure is 1.2 MPa. Firstly, the microstructures of low alloy steel are observed by optical microscope (OM) and scanning electron microscopy (SEM). Then, the electrochemical corrosion properties are studied by polarization curve and electrochemical impedance spectroscopy (EIS), and using Tafel fitting and equivalent circuit method, respectively. The corrosion surface morphology is characterized by SEM and energy-dispersive spectroscopy (EDS), Finally, the mutual relationship of rolling parameters, grain size, electrochemical parameters and corrosion surface morphology are discussed.

2. EXPERIMENTAL

2.1 Material and sample preparation

The influence of alloy elements on the corrosion performance is very important. Liu et al. [29] add alloy elements Al, Ni and Nb to improve strength and toughness. Yin et al. [28] add alloy element Mo to refine grain. Cu is an effective alloy element to enhance corrosion resistance [30]. Based on these analyses, the chemical composition of low alloy steel is shown in Table 1. Two kinds of samples by different thermo mechanical control process (TMCP) are obtained. The parameters are shown in Table 2. The electrochemical test specimen is cut into 10 mm × 10 mm × 3 mm, and the area of

exposure to the solution is 100 mm², other surfaces are isolated by epoxy resin. Before each test, the samples are ground with silicon carbide paper (grit: 600-1500), degreased with acetone, rinsed with distilled water and dried quickly in cold air to avoid oxidation. All samples are placed in a high pressure autoclave with 5 L capacity. The test solution with volume of 4 L is 3.5 wt% NaCl (analytical grade reagent) solution. N₂ is bubbled into the electrolyte for 3 h to deoxygenate, and H₂S/CO₂ mixture are purged into the autoclave for 1 h to saturate the solution. The electrolyte is heated to 75 °C and the total pressure is 1.2 MPa with partial pressure 0.09 MPa H₂S, 0.64 MPa CO₂ and 0.47 MPa N₂. After immersion test, specimens are removed from autoclave, and rinsed with deionized water. The samples are divided into two groups. The specimens in group one is used to analyze corrosion surface. The specimens in group two are used to perform electrochemical measurements.

Table 1. Chemical composition of low alloy steel (wt %)

C	Si	Mn	P	S	Al	Cr	Cu	W	Mo	Ni	Nb	Fe
0.085	0.24	1.36	0.006	0.002	0.04	0.23	0.16	0.21	0.21	0.11	0.012	balance

Table 2. TMCP rolling process parameters

Samples	start finish rolling temperature /°C	final rolling temperature /°C	final cooling temperature /°C	cooling rate /°C·s ⁻¹
No.1	856	840	638	10.4
No.2	851	835	612	15.9

2.2 Electrochemical measurements

The electrochemical measurements are performed by PATSTAT2273 workstation. The experiments are carried out using a conventional three-electrode cell, the platinum electrode as the auxiliary electrode, the saturated calomel electrode (SCE) as the reference electrode, and the low alloy steel as the working electrode. All polarization curves are obtained with scan rate of 0.1 mV/s. The EIS experiments are carried out at open circuit voltage using alternating current voltage amplitude of 8 mV and a frequency range is from 100 kHz to 0.1 Hz. The measurements are performed in aerated 3.5 wt% NaCl containing mixed gas H₂S, CO₂ and N₂ (1:7:5), the electrolyte is heated to 75 °C.

2.3 Morphology observation

The microstructures are observed using LEICA OM and FEI QUANTA 600 SEM. The electron back scattered diffraction (EBSD) are performed on FEI/Philips quanta 600 to investigate crystallographic characteristics maps and grain size. The surface morphologies are observed by SEM and EDS.

3. RESULTS AND DISCUSSION

3.1 Microstructure

Fig.1 shows the microstructures of low alloy steel. It can be seen that the type of microstructures is acicular ferrite ie., quasi polygonal ferrite, granular bainitic ferrite, and lath bainitic ferrite [31]. They are very similar to each other, polygon ferrite grain size is large, acicular ferrite distribution is relatively concentrated for No.1 steel. However, the ferrite grain of No.2 is relatively small, lath bainite are observed, which can be attributed to its faster cooling rate.

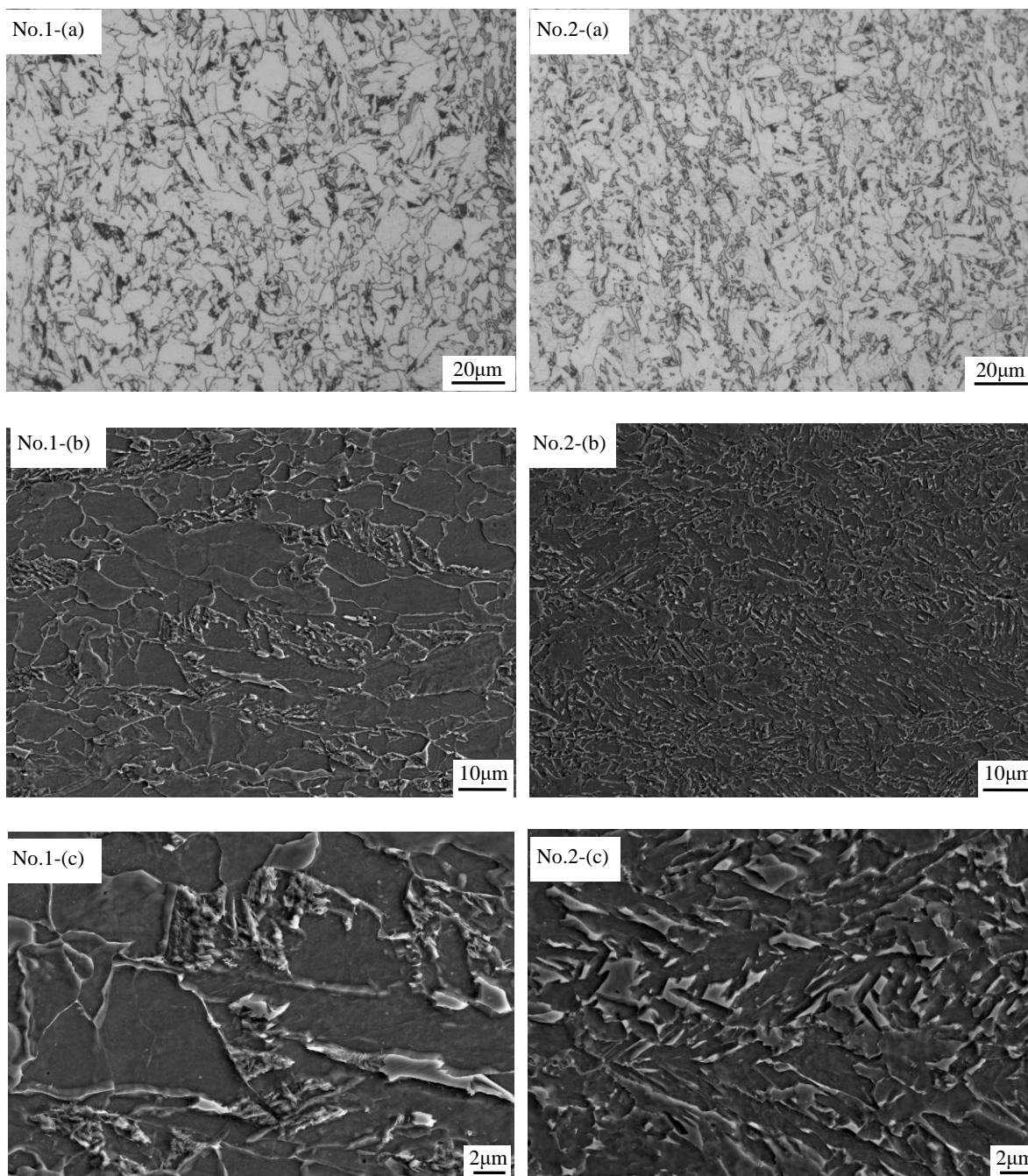


Figure 1. The microstructures of experimental steel showed by (a) OM, (b) and (c) SEM

Fig.2 shows that the area fraction of grain size. It is seen that the area fraction of fine ferrite grain size (grain diameter < 10 microns) for No.2 steel will much more than No.1 steel.

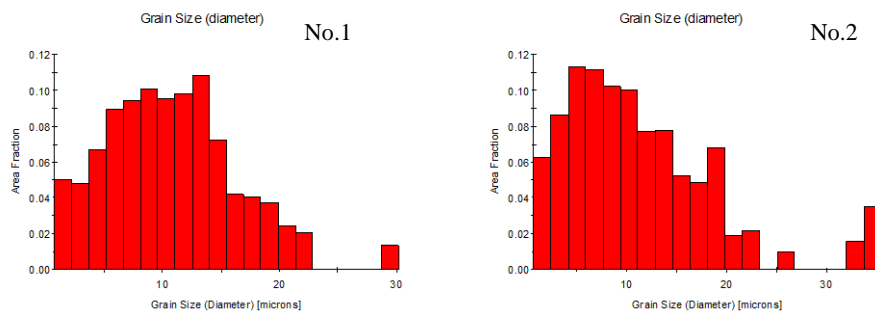


Figure 2. The relationship curve between grain size and area fraction for experimental steel

Under the same rolling temperature, ferrite grains are refined, granular bainite morphology becomes more obvious, the lath bainite have been found in No.2 steel. The reason may be that the transformation of granular bainite is a process of nucleation and growth, bainite nucleation rate will improve with cooling rate increases. But it is difficult to promote the granular bainite crystal nucleus to grow up, and the tiny and dispersion M/A islands come from untransformed austenite during acicular ferrite transformation are formed.

The grain boundaries orientation analysis is made by EBSD, as shown in Fig. 3.

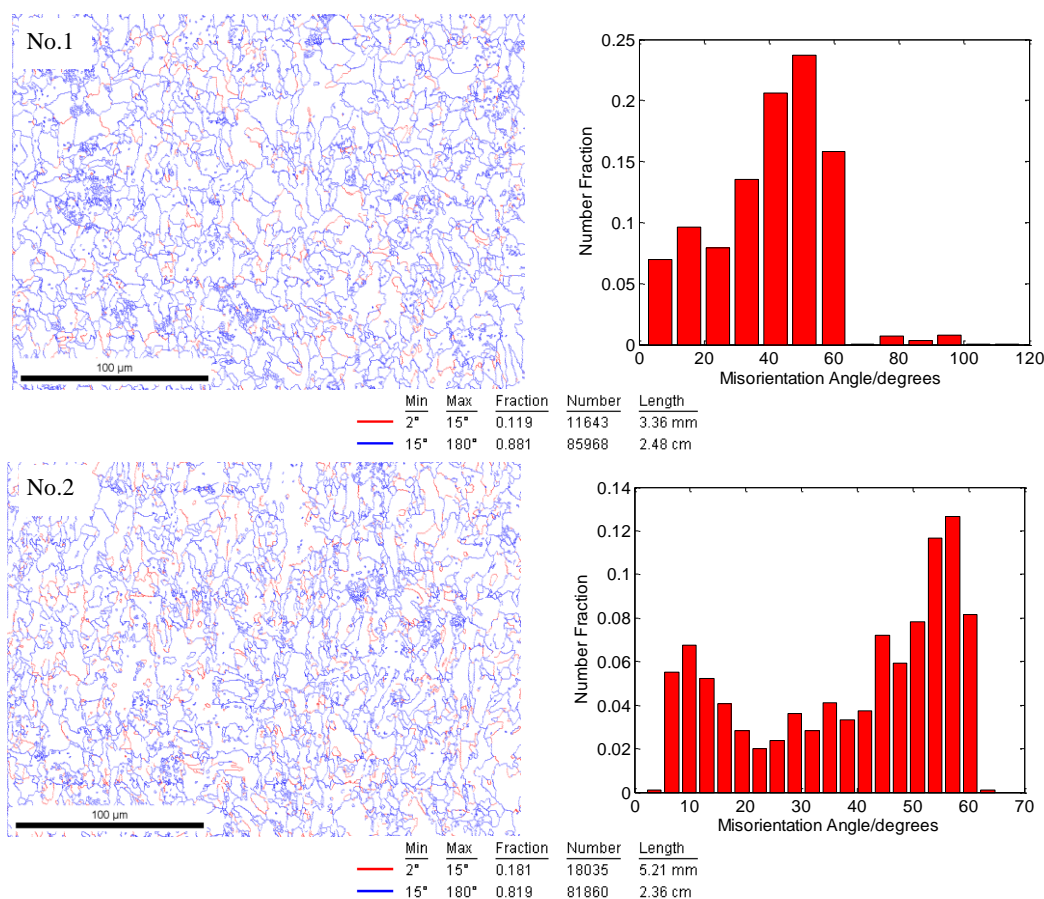


Figure 3. The EBSD analysis of experimental steel

The red line represents low misorientation boundaries of 2-15°, and the blue line stands for high misorientation boundaries of greater than 15°. It has been accepted that the grain boundary plays a key role on corrosion behavior, and low angle grain boundaries are usually more stable than high angle grain boundaries [32]. The microstructures of No.1 and No.2 are acicular ferrite, the area fraction of fine grain and low misorientation boundaries for No.2 is much more.

3.2 Potentiodynamic polarization curve measurement

To analyze the electrochemical corrosion properties depending on grain size and low misorientation boundaries. The typical polarization curves are shown in Fig.4. The corresponding anodic tafel constants (b_a), cathodic tafel constants (b_c), corrosion potential (E_{corr}), corrosion current density (I_{corr}) and polarization resistance (R_p) are shown in Table 3. The corrosion current density decreases simultaneously with immersion time increase from 96 h to 288 h, it will show denser corrosion product films are formed on Fe surface for 96 h. There are various species in the solution containing H_2S/CO_2 , such as H^+ , CO_3^{2-} , H_2CO_3 , HS^- , S^{2-} and H_2S , the surface corrosion is primarily dissolution of steel and formation of corrosion product film. So the corrosion mechanism is rather complicated [33]. The corrosion current density and polarization resistance are shown in Fig.5, it is found that there is an inverse relationship, the corrosion current density of No.2 steel is smaller than one of No.1 steel, which indicates corrosion resistance of No.2 steel is better than No.1 steel.

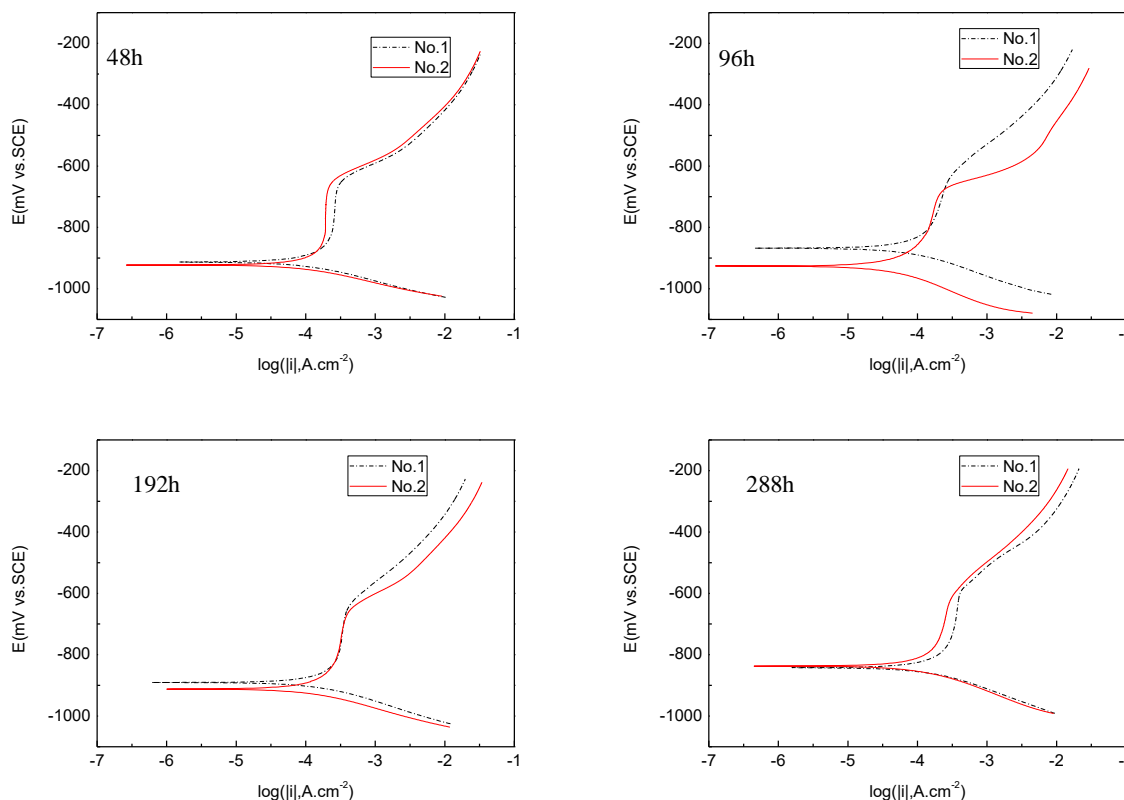


Figure 4. Potentiodynamic polarization curves of experimental steel in H_2S and CO_2 environment at $75^\circ C$ after immersion for 48 h, 96 h, 192 h and 288 h

Table 3. Potentiodynamic polarization parameters from a curve-fitting approach

Sample	Immersion time/hour	b_a (mV/dec)	b_c (mV/dec)	E_{corr} (mV vs.SCE)	I_{corr} (mA.cm ⁻²)	R_p (Ω .cm ²)
No.1	48	552	-69	-913	0.155	160.6
	96	487	-91	-868	0.116	264.4
	192	927	-84	-891	0.247	149.2
	288	923	-98	-842	0.258	129.8
No.2	48	882	-62	-923	0.143	166.7
	96	329	-108	-926	0.065	406.6
	192	481	-73	-912	0.170	250.4
	288	1024	-100	-837	0.187	197.6

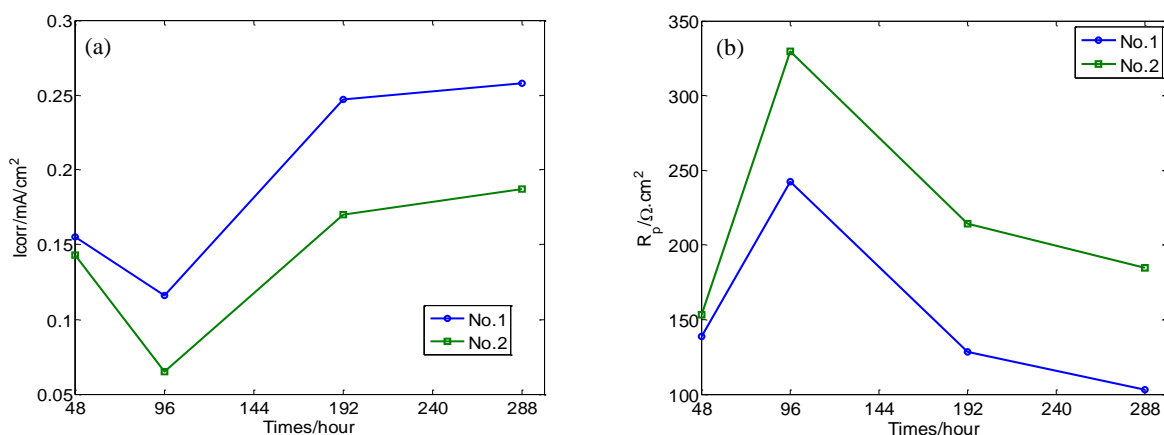


Figure 5. The fitting parameters of experimental steel in H₂S and CO₂ environment at 75°C after immersion for 48 h, 96 h, 192 h and 288 h (a) Corrosion current density vs. immersion time (b) Polarization resistance vs. immersion time

3.3 EIS measurement

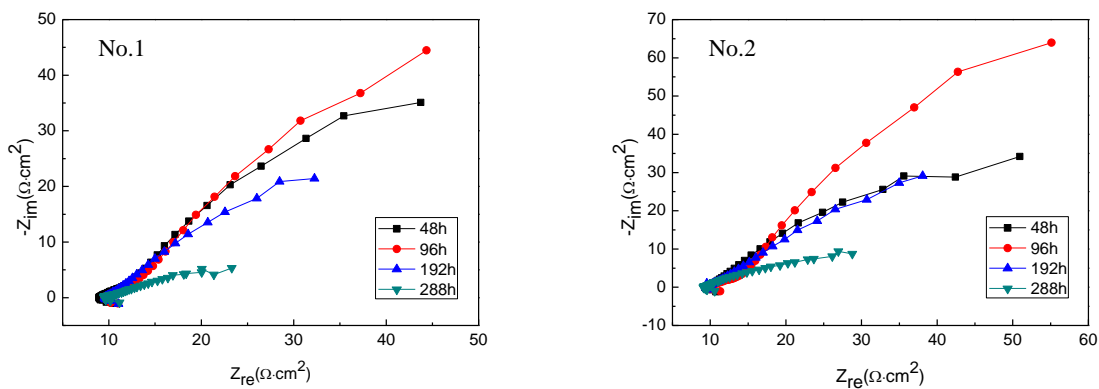


Figure 6. Nyquist plots of experimental steel in H₂S and CO₂ environment at 75°C after immersion for 48 h, 96 h, 192 h and 288 h

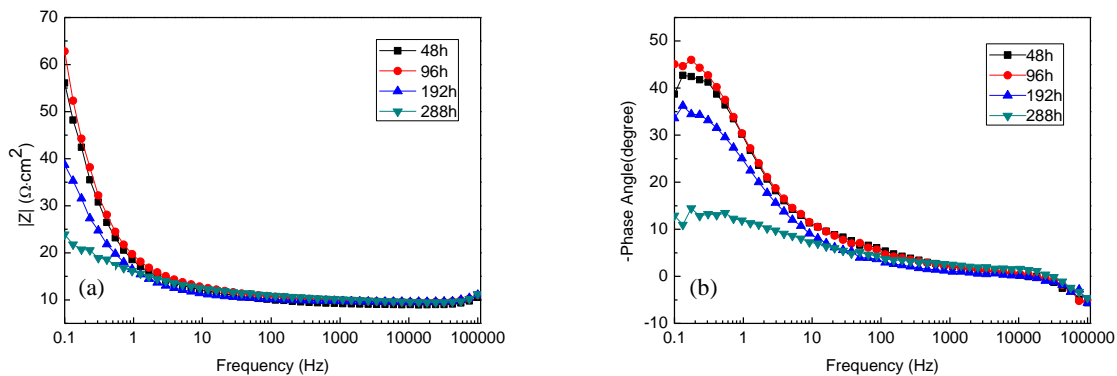


Figure 7. Bode diagrams of No.1 steel in H₂S and CO₂ environment at 75°C after immersion for 48 h, 96 h, 192 h and 288 h (a) The amplitude-frequency characteristic curve (b) The phase-frequency characteristic curve

EIS can obtain some information on corrosion processes that occur on electrode surface. The typical Nyquist diagrams are shown in Fig.6. Each spectrum includes an incomplete semicircle. The diameter of semicircle at low frequency decreases from 96 h to 288 h. Bode diagrams are shown in Fig.7 and Figure8.

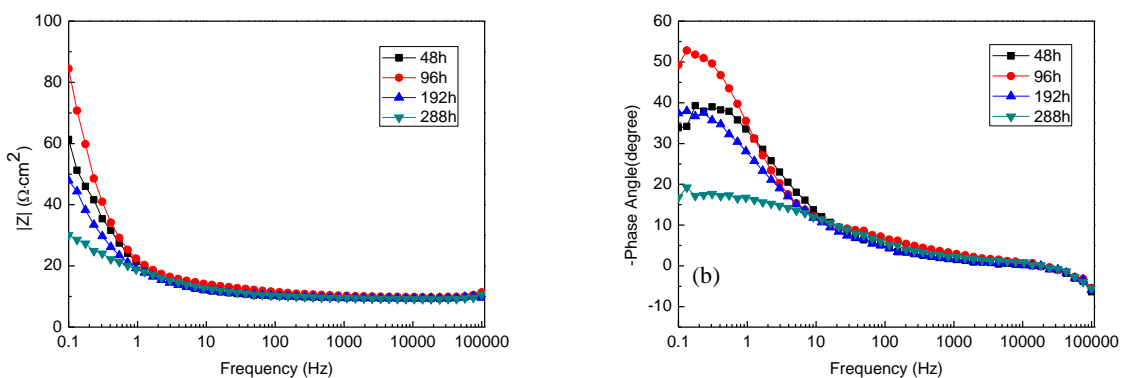


Figure 8. Bode diagrams of No.2 steel in H₂S and CO₂ environment at 75°C after immersion for 48 h, 96 h, 192 h and 288 h (a) The amplitude-frequency characteristic curve (b) The phase-frequency characteristic curve

f is frequency and $|Z|$ is impedance modulus. The impedance modulus define a straight line with a zero slope and phase angle remain in zero degrees at high frequency, which indicates a resistance is attributed, as commonly accepted to electrolyte resistance [34]. Bode plots show a capacitive-like behavior at the medium and low frequencies, characterize by a slanted impedance modulus and a phase angle defined maximum. The impedance modulus $|Z|$ at low frequency will gradually decrease from 96 h to 288 h, and impedance modulus $|Z|$ is biggest for No.2 after immersion 96 h, and the smallest one is for No.1 after immersion 288 h. As shown in Fig.7 (b) and Fig.8 (b), the broad-phase angle peak can show two time constants. So data are fitted by a simple electrical equivalent circuit depicted in Fig.9.

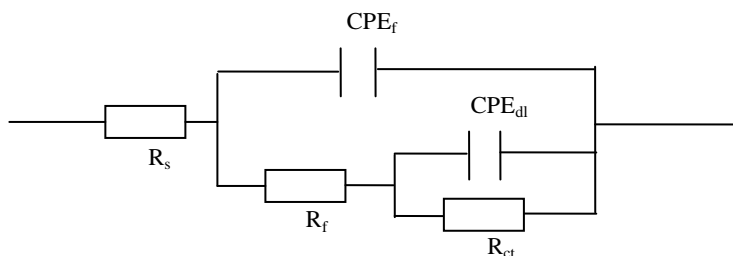


Figure 9. Equivalent circuits with two time constants

R_s represents electrolyte resistance between reference electrode and working electrode. R_f represents resistance of corrosion product film. R_{ct} represents charge transfer resistance, which is used to represent the difficulty of electrochemical reaction. Constant phase element (CPE) represents double-charge layer capacitance, which is expressed as follows.

$$Z_{CPE} = \frac{1}{Y_0(j\omega)^n} \tag{1}$$

where Y_0 is admittance, j is complex operator with $j = (-1)^{1/2}$, $\omega = 2\pi f$ is angular frequency, $n(0 < n < 1)$ is a dimensionless fractional exponent. CPE_f represents total surface electrode capacitance after electrode surface dispersion, n_1 is dispersion effect index of CPE_f , when $n_1 = 1$, CPE_f is equivalent to the ideal capacitance, when $n_1 = 0$, CPE_f is equivalent to the ideal resistance. CPE_{dl} represents capacitance for solution/metal surface in the corrosion hole, n_2 is dispersion effect index of CPE_{dl} . The total impedance Z can be rewritten as follows.

$$Z = R_s + \frac{1}{\frac{1}{R_f + \frac{1}{\frac{1}{Z_{CPE_{dl}} + R_{ct}}}} + \frac{1}{Z_{CPE_f}}} \tag{2}$$

Table 4 lists the fitting parameters.

Table 4. EIS fitting results of experimental steel

Sample	Immersion time/hour	R_s ($\Omega \cdot \text{cm}^2$)	Y_f ($\text{S} \cdot \text{sec}^n / \text{cm}$)	n_1	R_f ($\Omega \cdot \text{cm}^2$)	Y_{dl} ($\text{S} \cdot \text{sec}^n / \text{cm}^2$)	n_2	R_{ct} ($\Omega \cdot \text{cm}^2$)
No.1	48	9.172	0.005908	0.7367	4.469	0.01851	0.7726	134.1
	96	9.782	0.007821	0.688	5.116	0.02564	0.7679	237.4
	192	9.785	0.001657	0.9993	6.942	0.03466	0.6409	121.6
	288	9.776	0.000178	0.9998	8.558	0.03812	0.4364	94.5
No.2	48	9.577	0.001985	0.9076	4.643	0.01803	0.67	148.7
	96	10.11	0.01859	0.6415	7.632	0.00026	0.4783	322.1
	192	9.559	0.004662	0.7728	10.141	0.02413	0.6083	204.1
	288	9.342	0.003797	0.4199	19.128	0.02544	0.959	165.6

We can see that R_s changes rarely and the average value is about $9.64 \Omega \cdot \text{cm}^2$, which will show each test experiment is in a state of relative stability. R_f gradually increases and their changes are

small. The situation may be attributed to the fact that corrosion product films composed of iron sulfide and iron sulfide is electronically conductive [27]. The Y_{dl} are generally used to account for deviation caused by surface roughness, which will results in surface inhomogeneity on the microscopic level, such as porosity [31]. The Y_f fluctuates greatly from 96 h to 192 h, and the more obvious the fluctuation and the more serious the samples surfaces corrosion. The R_{ct} values will decrease from 96 h to 288 h, the largest value is obtained when immersion 96 h. Since both R_f and R_{ct} are resistances of corrosion process, the polarization resistance R_p ($R_p = R_{ct} + R_f$) is used to evaluate the corrosion rate, so there is inversely proportional relationship between corrosion current density i and polarization resistance R_p [35]. Fig.10 shows the polarization resistance curve. The obtained result by the EIS is consistent with those obtained by potentiodynamic polarization measurements from the Fig.5 (b) and Fig.10.

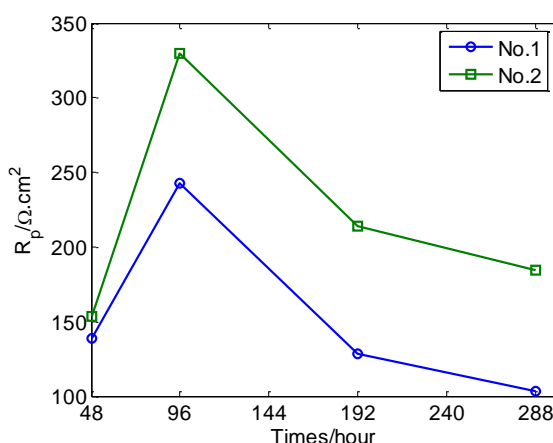
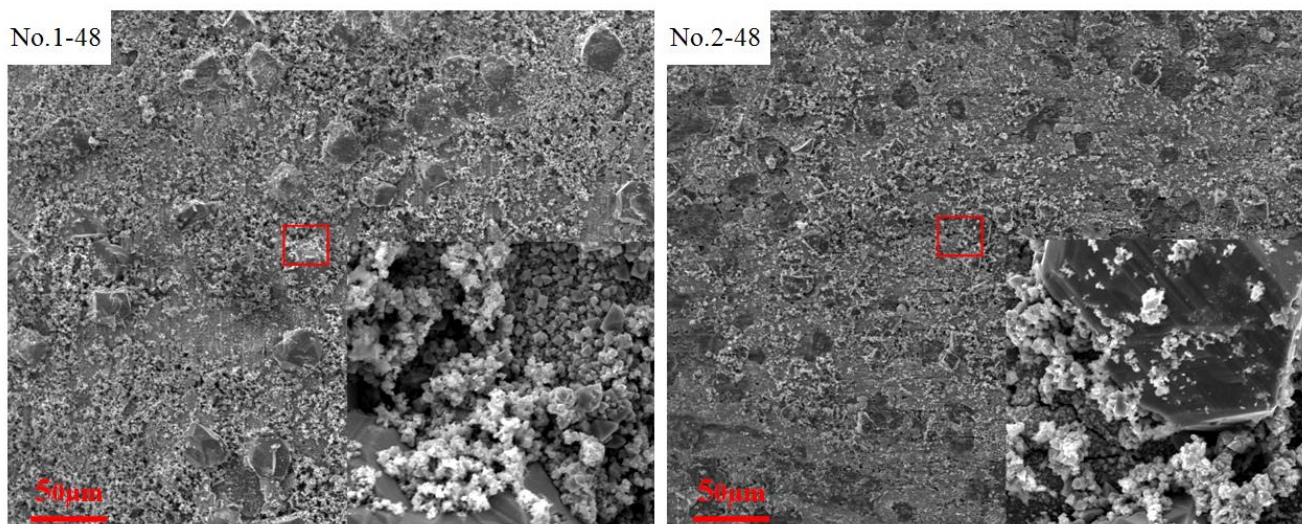


Figure 10. The polarization resistance R_p of experimental steel

3.4 Surface morphologies and composition analysis of corrosion product



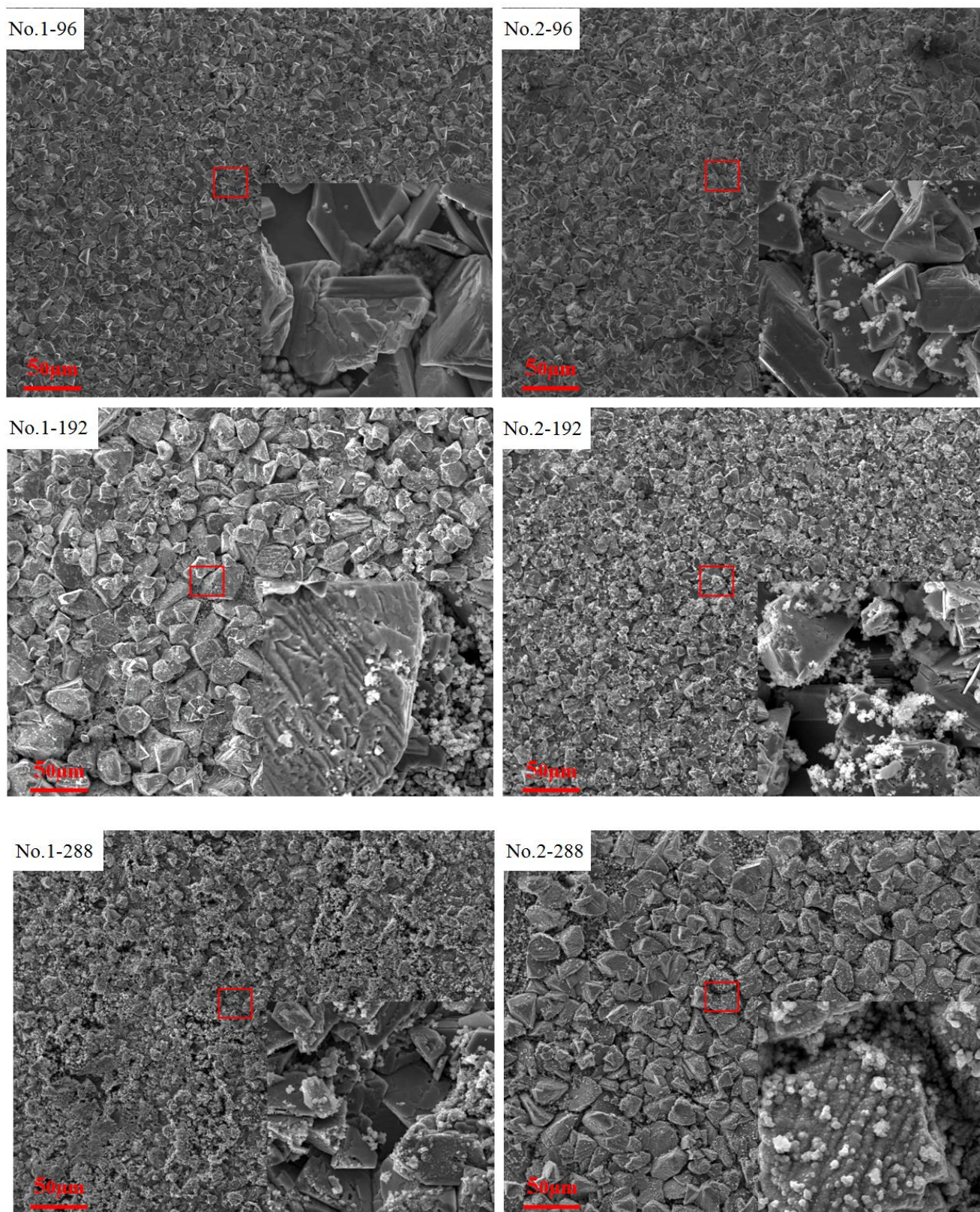


Figure 11. SEM images of corroded surface for No.1 and No.2 in H₂S and CO₂ environment at 75°C after immersion for 48 h, 96 h, 192 h and 288 h

Fig.11 shows the surface morphologies of experimental steel immersed in NaCl solution containing H₂S and CO₂. A lot of corrosion pits are found when immerse 48 h, it will become the source of local corrosion. Large particle size of corrosion products may be fall off or dissolved, there is not very compact film formed on the sample surface. However, the corrosion scales produced after immersion 96 h are very compact, it can protect steel matrix efficiently. The corrosion products after immersion 288h are loose, the gaps are possible to be passages that the corrosion solution diffuses into inner layer and even into substrate surface.

The No.1 and No.2 show the similar corrosion morphology in the whole reaction process, but corrosion products have a very big difference under the same test cycle. During the later corrosion period, it can be seen that the corrosion crystal size is very small and regular, combined with more closely, the structure of corrosion product film is complete. These will be easy to improve corrosion resistant performance.

Fig.12 shows the surface morphology and EDS of experimental steel after immersion 96h. The primary chemical elements of No.1 are iron, carbon, and sulphur. The primary chemical elements of No.2 are iron and sulphur. This indicates that the corrosion products are complexity compound containing different types of iron carbonate and iron sulfide. The peak number of No.2 is larger than the one of No.1 steel. This demonstrates that more iron sulfide is formed. This may result in No. 2 has good corrosion resistance.

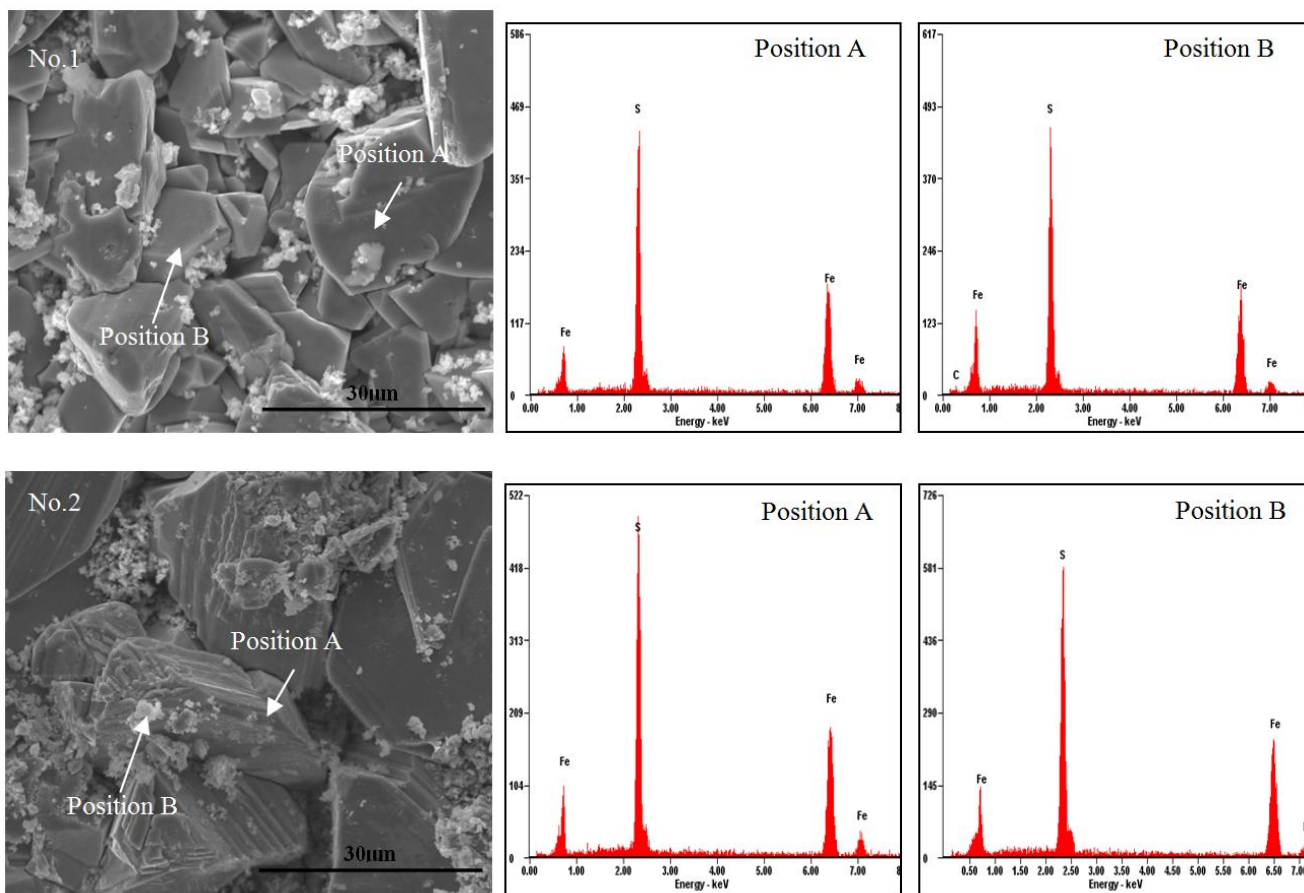


Figure 12. EDS of experimental steel in H₂S and CO₂ environment at 75°C after immersion 96h

4. CONCLUSIONS

The effects of grain size on corrosion properties of low alloy steel immersed in NaCl solution containing H₂S and CO₂ are investigated to simulate the the practical working environment of oil and gas industry. The conclusions are as follows:

- 1) The type of microstructure of low alloy steel is primarily acicular ferrite. The No.2 has the much finer ferrite grain size and lower angle grain boundary than No.1, which can be attributed to its faster cooling rate.
- 2) The corrosion current density of No.2 is smaller than No.1 with immersion time increases, and the polarization resistance of No.2 is much bigger than one of No.1 by potentiodynamic polarization and electrochemical impedance spectroscopy experiments, the average corrosion rate of No.2 is the lower than No.1. Combing with SEM and EDS, the results indicate that the corrosion resistance of No.2 is much more than No.1, and the pitting corrosion is not found under the harsh environment.
- 3) The number of Fe-S compounds peak of No.2 is larger than No.1. This indicates that more Fe-S compounds appear on the coupon surface, it can mitigate corrosion of low alloy steel to some extent, and the study would provide the basic knowledge of corrosion behavior of low alloy steel.

ACKNOWLEDGEMENT

This work was supported by the Science and Technology Project of Hebei Province (No.15211028), the Technology Support Project of Northeastern University at Qinhuangdao (No. XNK201604) and the Scientific Research Fund Project of Northeastern University at Qinhuangdao (No.XNB201717).

References

1. A. Chakma, *Energ. Convers. Manage.*, 38(1997)205.
2. B. Lemoine, Y. G. Li, R. Cadours, C. Bouallou and D. Richon, *Fluid Phase Equilib.*, 172(2000)261.
3. M. P. Cai, B. W. Strickler and A. A. Lizzio, *Carbon*, 38(2000)1757.
4. W. F. Li, Y. J. Zhou and Y. Xue, *J. Iron. Steel Res. Int.*, 19(2012)59.
5. X. H. Hao, J. H. Dong, J. Wei, W. Ke, C. G. Wang, X. L. Xu and Q. B. Ye, *Acta. Metall. Sin.*, 48(2012)534.
6. B. F. M. Pot, S. D. Kapusta and R. C. John, *In: corrosion 2002, Houston*, 2002.
7. X. H. Zhao, Y. Han, Z. Q. Bai, B. Wei, *Electrochim. Acta.*, 56(2011)7725.
8. L. D. Wang, H. B. Wu, Y. T. Liu, H. W. Zhang, L. F. Liu, D. Tang, *Mater. Sci. Technol.*, 21(2013)8.
9. E. Volpi, A. Olietti, M. Stefanoni, S. P. Trasatti, *J. Electroanal. Chem.*, 736(2015)38.
10. Y. Zou, J. Wang, Y. Y. Zheng, *Corros. Sci.*, 53(2011)208.
11. C. Yu, P. Wang, X. H. Gao, *Int. J. Electrochem. Sci.*, 10(2015)538.
12. S. Marcelin, N. Pébèr, S. Régnier, *Electrochim. Acta.*, 87(2013)32.
13. E. S. Sherif, *Int. J. Electrochem. Sci.*, 10(2015)34.
14. L. W. Wang, C. W. Du, Z. Y. Liu, X. X. Zeng, X. G. Li, *Acta. Metall. Sin.*, 47(2011)1227.
15. F. Farelàs, M. Galicia, B. Brown, S. Nesic, H. Castaneda, *Corros. Sci.*, 52(2010) 509.
16. M. Gao, X. Pang and K. Gao, *Corros. Sci.*, 53(2011)557.

17. N. Mundhenk, P. Huttenloch, R. Bäbeler, T. Kohl, H. Steger, R. Zorn, *Corros. Sci.*, 84(2014)180.
18. J. H. Ding, L. Zhang, M. X. Lu, J. Wang, Z. B. Wen, W. H. Hao, *Appl. Surf. Sci.*, 285(2014)33.
19. P. P. Bai, S. Q. Zheng, C. F. Chen, *Mater Chem Phys*, 149(2015)295.
20. A. C. Tobón¹, M. D. Cruz¹, J. L. G. Velázquez¹, J. G. G. Salcedo¹, R. M. Salinas, *Int. J. Electrochem. Sci.*, 9(2014)6781.
21. M. A. Veloz, I. González, *Electrochim. Acta.*, 48(2002)135.
22. L. Q. Chen, J. Zhou, Y. X. Chen, P. P. Bai, J. Wu, S. Q. Zheng, *Int. J. Electrochem. Sci.*, 11(2016)3987.
23. G. A. Zhang, Y. Zeng, X. P. Guo, *Corros. Sci.*, 65(2012)37.
24. H. B. Wu, L. F. Liu, L. D. Wang, Y. T. Liu, *J. Iron. Steel Res. Int.*, 21(2014)76.
25. Q. Y. Wang, X. Z. Wang, H. Luo, J. L. Luo, *Surf. Coat Tech.*, 291(2016)250
26. H. W. Wang, P. Zhou, S. W. Huang and C. Yu, *Int. J. Electrochem. Sci.*, 11(2016)1293.
27. W. Y. P. K. Zhu, J. G. Deng, *Int. J. Electrochem. Sci.*, 11(2016) 9542.
28. Z. F. Yin, W. Z. Zhao, Z. Q. Bai, Y. R. Feng and W. J. Zhou, *Electrochim. Acta.*, 53(2008)3690.
29. M. Liu, J. Q. Wang, W. Ke and E. H. Han, *J. Mater. Sci. Technol*, 30(2014)504.
30. F. L. Sun, X. G. Li and F. Zhang, *Acta. Metall. Sin.*, 26(2013) 257.
31. L. Fan, D. H. Zhou, T. L. Wang, S. R. Li and Q. F. Wang, *Mater. Sci. Eng., A*, 590(2014) 224.
32. L. Lapeire, E. Martinez, K. Verbeken, I. Graeve, L. Kestens and H. Terryn, *Corros. Sci.*, 67(2013) 179.
33. H. Y. Ma, X. L. Cheng and G. Q. Li, *Corros. Sci.*, 42(2000) 1669.
34. S. Fajardo, D. M. Bastidas, M. Criado and J. M. bastidas, *Electrochim. Acta.*, 129(2014)160.
35. S. W. Kim and H. W. Lee, *Int. J. Electrochem. Sci.*, 9(2014)4709.

© 2017 The Authors. Published by ESG (www.electrochemsci.org). This article is an open access article distributed under the terms and conditions of the Creative Commons Attribution license (<http://creativecommons.org/licenses/by/4.0/>).